Journal of Medicinal Chemistry

Article

Synthesis, Biological Evaluation, and 3D QSAR Study of 2-Methyl-4-oxo-3-oxetanylcarbamic Acid Esters as N-Acylethanolamine Acid Amidase (NAAA) Inhibitors

Stefano Ponzano, Anna Berteotti, Rita Petracca, Romina Vitale, Luisa Mengatto, Tiziano Bandiera, Giovanni Bottegoni, Fabio Bertozzi, Daniele Piomelli, and Andrea Cavalli

J. Med. Chem., **Just Accepted Manuscript** • DOI: 10.1021/jm501455s • Publication Date (Web): 07 Nov 2014

Journal of Medicinal Chemistry is published by the American Chemical Society. 1155 Sixteenth Street N.W., Washington, DC 20036

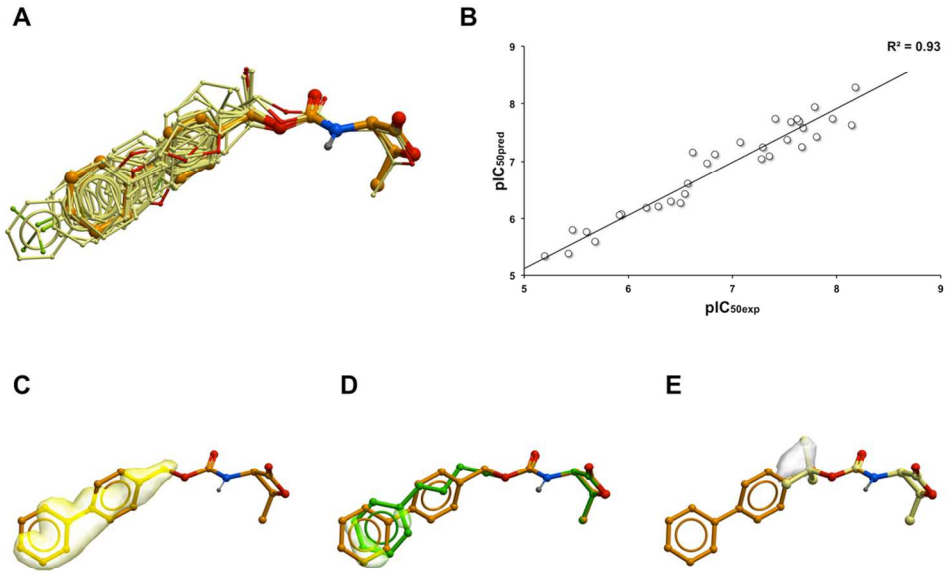

Figure 2. A: The overlay of the training set molecules superimposed to compound 2; B: Correlation plot between pIC50exp and pIC50pred; C: In licorice the 3D structure of 2 is reported. The transparent blobs are the equipotential contours of the lipophilic 3D QSAR APF component. The grey region represents the ideal lipophilic shape for NAAA inhibition. D: In green is reported the 3D structure of 20 superimposed to compound 2, in orange. The grey blobs represent the equipotential contours of the Sp2 hybridization 3D QSAR APF component. The occupancy of such regions is detrimental for the potency. E: In yellow is reported 16 superimposed to compound 2, in orange. The grey blobs represent the equipotential contours of the size 3D QSAR APF component. The occupancy of such regions is detrimental for the potency.
177x123mm (300 x 300 DPI)

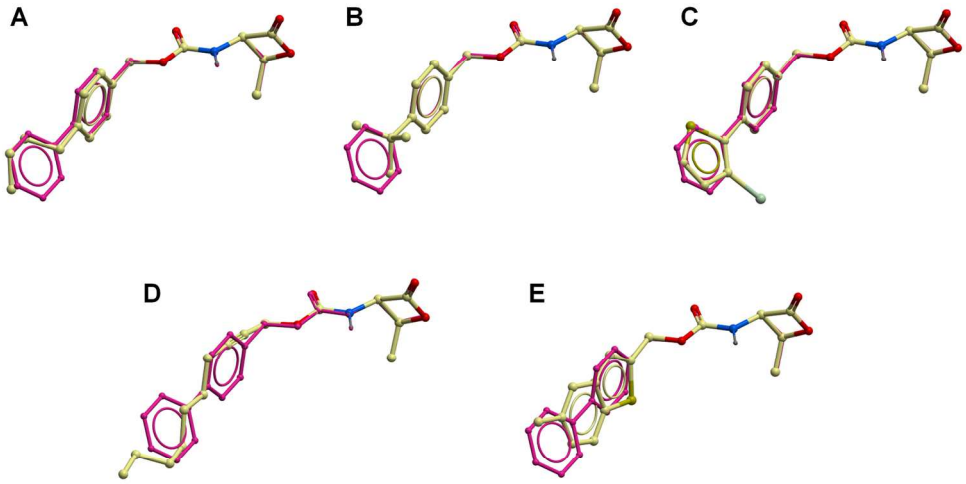

Figure 3: The molecules selected for the validation of the 3D QSAR model are shown in yellow, as licorice, superimposed to 2 in pink. A: molecule 9r, B: molecule 9s, C: molecule 9t, D: molecule 9v, E: molecule 9u. 177x123mm (300 x 300 DPI)

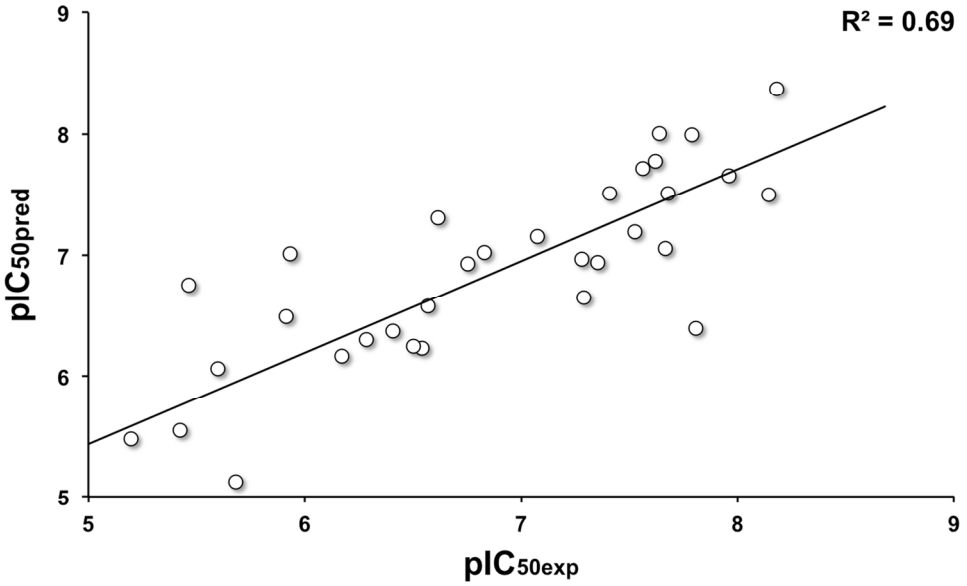

Correlation plot between the experimental pIC50 and the leave-one-out cross-validated pIC50.
177x108mm (300 x 300 DPI)

Synthesis, Biological Evaluation, and 3D QSAR Study of 2-Methyl-4-oxo-3-oxetanylcarbamic Acid Esters as *N*-Acylethanolamine Acid Amidase (NAAA) Inhibitors

Stefano Ponzano,[†,#] Anna Berteotti,[†,#] Rita Petracca,[†] Romina Vitale,[†] Luisa Mengatto,[†] Tiziano Bandiera,[†] Giovanni Bottegoni,[†,] Fabio Bertozzi,[†,*] Daniele Piomelli,[†,§] Andrea Cavalli[†,‡]*

[†]Drug Discovery and Development, Istituto Italiano di Tecnologia, Via Morego 30, I-16163 Genova, Italy

[§]Departments of Anatomy and Neurobiology, Pharmacology and Biological Chemistry, University of California, Irvine, California 92697-4621, United States

[‡]Department of Pharmacy and Biotechnology, University of Bologna, Via Belmeloro 6, I-40126 Bologna, Italy

Abstract

N-(2-oxo-3-oxetanyl)carbamic acid esters have recently been reported to be noncompetitive inhibitors of the *N*-acylethanolamine acid amidase (NAAA) potentially useful for the treatment of pain and inflammation. In the present study, we further explored the structure activity relationships of the carbamic acid ester side chain of 2-methyl-4-oxo-3-oxetanylcarbamic acid ester derivatives. Additional favourable features in the design of potent NAAA inhibitors have been found together with the identification of a single digit nanomolar inhibitor. In addition, we devised a 3D QSAR using the Atomic Property Field method. The model turned out to be able to account for the structural variability, and was prospectively validated by designing, synthesizing, and testing novel inhibitors. The fairly good agreement between predictions and experimental potency values points to this 3D QSAR model as the first example of quantitative structure activity relationships in the field of NAAA inhibitors.

Introduction

The fatty-acid ethanolamides (FAEs) are a class of multi-functional lipid mediators that have attracted significant attention due to their potential role in physiological and pathological processes including pain,[1-3] innate immunity,[4] reward regulation[5] and feeding.[6, 7] In particular, palmitoylethanolamide (PEA), the endogenous amide of palmitic acid and ethanolamine, has been shown to inhibit peripheral inflammation and mast cell degranulation[8, 9] and to exhibit antinociceptive properties in rat and mouse models of acute and chronic pain.[10-12] Furthermore PEA has been indicated to attenuate skin inflammation[13, 14] and neuropathic pain in humans.[15] These effects are mainly attributed to the ability of PEA to activate peroxisome proliferator-activated receptor-α (PPAR-α), a member of the steroid/nuclear receptor superfamily.[1, 2, 7, 16]

PEA is deactivated into free palmitic acid and ethanolamine by two intracellular lipid amidases: fatty acid amide hydrolase (FAAH), which prefers anandamide over PEA and OEA,[17] and *N*-acylethanolamine acid amidase (NAAA), the main responsible for PEA cleavage.[18-20]

In this light, selective NAAA inhibitors could represent a viable strategy to raise local levels of PEA, potentially leading to anti-inflammatory and analgesic effects via PPAR-α signaling.[1, 2, 7] Only a restricted number of NAAA inhibitors, belonging to a narrow range of chemical classes, has been reported so far.[21, 22] Generally most of the first discovered compounds have been shown to block the enzyme hydrolytic activity with micromolar potencies.[23-27] Rational drug discovery efforts aimed at either identifying novel scaffolds or at improving already known ones have been severely hampered by the limited amount of detailed structural information on this target.

NAAA is a cysteine hydrolase that belongs to the *N*-terminal nucleophile (Ntn) family of enzymes. [20, 28, 29] Like other Ntn enzymes, NAAA is produced as an inactive proenzyme and is activated at acidic pH by autocatalytic cleavage at a specific site of the peptide chain.[30]

Recently, a comparative model of NAAA active site was generated starting from the coordinates of conjugated bile acid hydrolase (CBAH).[31] The insights gained from this model eventually led to the discovery of the serine-derived 2-oxo-3-oxetanylamide, (*S*)-OOPP, as a first sub-micromolar NAAA inhibitor. The model turned out to be consistent with both mutagenesis data, explaining the role of several residues in the catalytic process, as well as with the SAR exploration performed around the newly identified potent NAAA inhibitors, featuring an α-amino-β-lactone ring as a reactive electrophilic warhead.[32]

Structure-activity relationship (SAR) studies of α-amino-β-lactone derivatives, as carbamic acid esters, investigated the effects on NAAA inhibition of side chain modifications and the stereo-chemical requirements of the introduction of a β-substitution.[33-35] These works led to the identification of compounds that were highly potent at inhibiting both rat and human NAAA, such as β-lactones **1** (**ARN077**)[33, 34, 36] and **2**[34] (Figure 1). The β-lactone ring of these compounds was proved to be responsible for the inhibition mechanism, interacting covalently with the *N*-terminal catalytic cysteine (Cys126), through the formation of a thioester bond.[36]

In the present study, we further extended the exploration of the SAR for this class of inhibitors focusing on the carbamic acid ester side chain. Besides generating new compounds, a more extensive investigation of the structural determinants for NAAA activity could also contribute to shed light on some three-dimensional features of NAAA binding pocket, thus facilitating future development of new molecular scaffolds.

To this aim, combining previously reported results[34] together with data on 17 new compounds purposely synthesized to enhance the structural diversity of the set, we devised a three-dimensional Quantitative Structure-Activity Relationship (3D QSAR) model. Our model was built adopting the recently reported Atomic Property Field (APF) method.[37] APF can be described as a grid-based model in which the discrete features of a classic pharmacophore are replaced by continuous, regularly spaced three-dimensional lattices. Each molecule from our training set contributed to this composite set of grids proportionally to its reported activity. With respect to more traditional approaches, the main advantage of this technique is that the strength of the overlap between a new putative compound and the APF signature of the template molecules can be directly translated into a prediction of activity. Finally, our model was prospectively validated. Based on the predictions generated on a list of virtual compounds, we selected 5 high-scoring derivatives to be actually synthesized and tested. Notably, the activities of the prospectively tested compounds turned out to be in line with the predictions.

Chemistry

Novel 2-methyl-4-oxo-3-oxetanylcarbamic acid esters **9a–v** (Table 1 and Table 4) were synthesized using previously reported synthetic protocols (Scheme 1).[34, 35] First, alcohols **3** were activated either as imidazole 1-carboxylates **4** or as a mixture of 2-pyridyl carbonates **5** and 2-oxopyridine-1-carboxylates **6**. The desired final 2-methyl-4-oxo-3-oxetanylcarbamic acid esters **9a–v** were obtained either by reaction of (2*S*,3*R*)-2-methyl-4-oxo-3-oxetanylammonium toluene-4-sulfonate (**7**) with compounds **4–6** or by cyclization of intermediate α-substituted-β-hydroxycarboxylic acids **8**, synthesized from commercially available *D*-threonine and the corresponding activated alcohols **4–6**.

Most of the alcohols used in the above mentioned methodologies were commercially available or obtained *via* reduction of the corresponding commercially available carboxylic acids. Alcohols **3c–e**,**p** were prepared as reported in Scheme 2. While the oxetane derivative **3c** was synthesized in a straightforward manner from oxetan-3-one (**10**) by reaction with butyl lithium, compound **3d** was obtained in a one pot procedure starting from 4-bromobutylbenzene (**11**), which was first converted into its lithium analogue and subsequently reacted with **10**. The syntheses of alcohols **3e** and **3p** were accomplished according to literature procedures. The commercially available 2-methylpropanoic acid (**12**) was reacted with (2-bromoethyl)-benzene using sodium hydride and *in situ* prepared lithium diisopropylamine to afford the carboxylic acid **13**.[38] Lewis acid addition (boron trifluoride diethyl etherate) to a mixture of ethyl 4-hydroxybenzoate (**14**) and cyclohexene afforded the ester **15**.[39] Both intermediates **13** and **15** were submitted to lithium aluminium hydride reduction to furnish the desired alcohols **3e** and **3p**.

Results and Discussion

The main objectives of the present study were to *i)* perform an extended structural exploration specifically tailored on the side chain of 2-methyl-4-oxo-3-oxetanylcarbamic acid ester derivatives, *ii)* exploit this structural variability to devise a 3D QSAR model, and *iii)* prospectively validate the model by synthesizing novel active compounds in line with the predictions.

SAR study

Starting from previously identified compound **1**,[33, 34, 36] extensive SAR studies led to the discovery of the first single-digit nanomolar inhibitor of intracellular rat (and human) NAAA activity **2**.[34] Here, a new series of 2-methyl-4-oxo-3-oxetanylcarbamic acid esters **9a**–**q** (Table 1) were synthesized to verify additional features, which could help confirm or better define the structural determinants for NAAA activity. We therefore explored the effect on NAAA inhibition of different side-chains taking into account structural modifications, such as the introduction of heteroatoms, the length of the side-chain, and the di-substitution in α and β position with respect to the carbamic acid function. Finally, to further define the contribution of conformationally constrained moieties, more rigid structures based on the tridimensional shape of **2** were taken into consideration.

The potency of the new synthesized 2-methyl-4-oxo-3-oxetanyl carbamic acid esters **9a**–**v** was evaluated by their ability to inhibit the hydrolysis of 10-cis-heptadecenoylethanolamide (an unnatural FAE) by native NAAA prepared from rat lungs. Median inhibitory concentration (IC_{50}) values obtained using the rat enzyme (*r*-NAAA) are reported in Table 1 and Table 4.

Previously described analogues (**1**,**2** and **16**–**29**)[34] and their corresponding *r*-NAAA inhibitory activity are reported in Table S1 (see Supporting Information).

The analysis of the IC_{50} values reported in Table 1 together with those of the previously reported analogues (Table S1) allows some general considerations to be made. The introduction of a fluorine atom in the para position of the phenyl ring (**9a**, IC_{50} = 0.24 μM) was detrimental for the activity, leading to a ca. 5-fold drop in potency compared to **1** (Table S1). Taking into consideration possible modifications on compound **22** (IC_{50} = 0.76 μM, Table S1), a substitution of a methyl group with a more lipophilic chlorine atom (**9b**) resulted in an increased inhibitory potency (IC_{50} = 0.28 μM), while the introduction of an oxetane moiety in α-position with respect to the carbamate (**9c**) turned out to be detrimental for activity (IC_{50} = 3.76 μM).

The same negative effect of a di-substitution in the α-position to the carbamate was observed in analogue **9d** (IC_{50} = 0.52 μM) compared to **1**, therefore indicating a limited space in the region of the enzyme proximal to the carbamic function. A similar loss in activity was observed with the insertion of a *gem*-di-methyl substitution in the β-position as for compound **9e** (IC_{50} = 3.43 μM), which resulted 9-fold less active than the corresponding unsubstituted analogue **20** (IC_{50} = 0.39 μM, Table S1).

Whereas the presence of a terminal cyclohexyl moiety in a four carbon atoms aliphatic linker (**9f**) retained approximately the same potency as for the previously reported 5 carbon atom aliphatic linker analogue **28** (IC_{50} = 0.013 μM, Table S1), a ca. 300-fold loss in activity was observed when the cyclohexyl moiety was directly connected to the carbamic acid function (**9g**, IC_{50} = 5.42 μM).

The addition of a methylene unit to the aliphatic linker of **1**, leading to a 6 carbon atom alkyl chain, was reported to be detrimental for activity (**21**, IC_{50} = 1.17 μM, Table S1), whereas the insertion of an additional carbon atom (**9h**) surprisingly restored the original activity (IC_{50} = 0.039 μM). A short alkylic chain bearing a terminal *p*-methylphenyl group (**9i**, IC_{50} = 1.22 μM) confirmed a low μM activity as previously observed for the phenethyl derivative (**18**, IC_{50} = 1.22 μM, Table S1).

To further investigate and possibly confirm the importance of the rigidity of the side chain for potent enzyme inhibition, new β-lactones structurally related to **2** were designed and tested against *r*-NAAA. The substitution of the proximal phenyl ring with an acetylene functionality (**9j**), which retains the overall shape of the side chain of **2**, led to a 3-fold drop in potency. The same variation in activity was observed when substituting the terminal phenyl ring with a thiophene moiety (**9k**, IC_{50} = 0.022 μM), whereas the substitution with a cyclohexyl moiety (**9l**, IC_{50} = 0.007 μM) resulted in a compound equally active to **2** (Table S1). To the best of our knowledge, compounds **2** and **9l** are the most active, single-digit nanomolar NAAA inhibitors so far reported in literature.

We then evaluated the effect of small substituents at para position of the biphenyl moiety. No significant variation in potency was observed for the *p*-fluoro derivative **9m** (IC_{50} = 0.011 μM), while a methyl or trifluoromethyl group in the same position led to slightly less potent compounds (**9n** and **9o**, IC_{50} = 0.029 μM and IC_{50} = 0.036 μM, respectively). Interestingly, increasing the flexibility of the side chain of compound **9l** by insertion of an oxygen atom between the phenyl and cyclohexyl ring (**9p**) led to only a 3-fold decrease in activity (IC_{50} = 0.023 μM). Finally, replacing the *p*-biphenyl ring with a more polar, fused bicyclic piperonyl moiety (**9q**) led to a 25-fold drop in potency.

3D QSAR model

We assembled a training set encompassing 33 compounds: 17 new, purposely synthesized 2-methyl-4-oxo-3-oxetanylcarbamic acid esters derivatives (Table 1) and 16 analogues taken from a previous SAR study (Table S1).[34] The 3D QSAR model was built using the APF approach, namely a continuous 3D pharmacophoric potential implemented on a set of regularly spaced grids.[37] This multi-component 3D potential was generated solely by the training set compounds, each individual contribution reflected preferences for various atomic properties at each point in space, and it was rescaled according to the

compound's experimental potency. Multiple ligands consistently displaying atoms with similar properties in the same location generated a strong pharmacophoric signal for these common features. In line with the original APF 3D-QSAR implementation proposed by Totrov,[37] we selected seven properties to be analyzed and assigned: charge, hydrogen bond donor propensity, hydrogen bond acceptor propensity, sp^2 carbon atom hybridization, and lipophilicity, to encompass the classic pharmacophoric features, plus two more unconventional properties, namely size and electropositivity/negativity, to take into account more subtle differences among substituents that would have been very difficult to capture otherwise.

First, the training set compounds were superimposed using, as template, the transition state model of compound **2**, as previously obtained by quantum chemical calculations (see Experimental Section for details).[34] In Figure 2A, the structural alignment of the training set compounds is reported. As expected, the β-lactone ring perfectly matched. Conversely, the conformational arrangement of the side chains captured the diversity of the training set and represented the truly informative core of our model. For each molecule, a seven-component property vector was evaluated and used to generate the 3D QSAR model. The optimal number of latent vectors to be used in the partial least square (PLS) analysis was selected in order to optimize the overall squared correlation coefficient between the predicted and the observed activities (R^2) as well as the leave-one-out cross-validation results (Q^2) on the training set.

In Table 2, R^2 and Q^2 values as a function of the number of latent vectors are reported. Eventually, we decided to use 6 latent vectors meeting the generally accepted threshold of 1 latent vector for every 5 compounds employed in the training set.[40] In this way, our model showed a good R^2 coefficient between the experimental pIC_{50} (pIC_{50exp}) and the predicted pIC_{50} (pIC_{50pred}), ($R^2 = 0.93$, see Figure 2B), and a good predictivity with a $Q^2 = 0.69$ (see Figure S1).

In Table 3, the experimental, predicted, and leave-one-out cross-validated pIC_{50} values for the training set are reported.

The structural implication of the generated 3D QSAR model can be visualized in terms of isopotential contour maps of the various APF components. For example, the lipophilicity field of the model was useful to pinpoint regions that react to the presence of a lipophilic moiety, enhancing or reducing the inhibitory potency. As already reported, the size and the shape of the lipophilic tail are key determinants for the inhibitory potency of the β-lactones compounds.[32-34] In Figure 2C, only the regions in which a lipophilic moiety improved NAAA inhibition are reported. Interestingly, the structural implications of the proposed model are in agreement with those proposed by Solorzano and colleagues by means of mutagenesis and homology modeling studies (see also the covalent docking studies and Figure S2 in Supporting Information).[31] The shape of this lipophilic region suggests a preference for linear moieties in the carbamic acid esters for optimal enzyme recognition. The sp^2 hybridization atomic property field generated by the training set is reported in Figure 2D. In particular, the regions in which the presence of sp^2 hybridized atoms was detrimental for the inhibitory potency are shown. For example, a terminal cyclohexyl moiety in a four units aliphatic linker was preferred to a terminal phenyl ring, as confirmed by the drop in potency of **20** with respect to compound **9f**. In Figure 2E, the regions in which large substituents led to a drop in the inhibitory potency are reported. This seems to suggest that the access to the lipophilic subpocket is quite tight and, as such, ill-suited to lodge bulky substituents like the *tert*-butyl group of compound **16**.

Model validation

The 3D QSAR model was then challenged by designing, synthesizing, and testing novel compounds. An in silico library of 200 β-lactones derivatives was assembled starting from a list of commercially available alcohols. Their activity data were predicted through the 3D QSAR model (pIC_{50pred}) and the

compounds were then ranked accordingly. The compounds with a $pIC50_{pred}$ value greater or equal to 7.45 were selected for visual inspection. The structures of the resulting 23 compounds along with pIC_{50pred} values are reported in Table S2 (see Supporting Information). Eventually, we selected 5 new derivatives for chemical synthesis and biological evaluation. The selection was based on the following criteria: *i)* good predicted activity (rank), *ii)* chemical feasibility, *iii)* actual availability of the alcohol substituent, *iv)* introduction of new chemical features with respect to already known β-lactones NAAA inhibitors. The compounds (**9r**–**v**) were synthetized according to Scheme 1, and their rank and activity data are reported in Table 4. For comparison, in Table S3 (see Supporting Information) we also report the structures of the five least active compounds as predicted by the model.

It clearly emerges the quite good agreement between predicted and observed pIC_{50} values, further highlighting the robustness of the present 3D QSAR model. Indeed, our model not only retrospectively explained the SAR in the lipophilic region of the NAAA binding pocket, but could also be used prospectively to design novel NAAA inhibitors.

In Figure 3, the novel compounds are reported. The new molecules showed a good superimposition with respect to the biphenyl moiety of **2**. In particular, the APF lipophilic contribution of these molecules matched well with the ideal lipophilic shape and size of the side chain obtained by our model. These compounds were not profoundly different from those used in the training set to devise the model. In this regard, it should be pointed out that a hopping exercise aimed at identifying completely novel chemical scaffolds was outside the scope of the present 3D QSAR study. Furthermore, given the covalent nature of the interaction established by these compounds with the enzyme,[36] fair activity predictions based on structure can only be limited to compounds sharing the same mechanism of covalent inhibition. However, each new compound displayed a new structural feature, which incrementally expanded our knowledge of the shape of the pocket, particularly relevant also in light of

the lack of a NAAA crystal structure to be utilized in structure-based studies. Compound **9r** (Figure 2A; IC_{50} = 0.015 μM, Table 4) displays an activity only marginally lower with respect to **2** (IC_{50} = 0.007 μM, Table S1) and **9l** (IC_{50} = 0.007 μM, Table 1), confirming that in this region an aliphatic group is well tolerated and suggesting that more flexible non-ring substituents can be explored. In Figure 3B, compound **9s** (IC_{50} = 0.022 μM, Table 4) is reported. Although the molecule resembles the lipophilic signature of **2,** the presence of a *tert*-butyl substituent in para to the phenyl ring was not detrimental for potency, indicating that, in this position, a bulky substituent is well tolerated. This was also confirmed by the potency displayed by compound **9t** (Figure 3C, IC_{50} = 0.028 μM, Table 4) with the bromo-substituted thiophene ring matching the lipophilic map of the present model while, at the same time, exploring an additional volume by means of the bromine substituent. On the same line, compound **9v** was characterized by a reasonable activity (IC_{50} = 0.077 μM, Table 4) combining a flat, sp^1 group in the region proximal to the carbamate, as already seen in **9j**, with a long aliphatic chain (Figure 3D). Compound **9u** represented an interesting exercise by which we explored the possibility to introduce a heteroaromatic ring in close proximity to the carbamate functionality (Figure 3E). Interestingly, this compound turned out to be very active (IC_{50} = 0.013 μM, Table 4). When combined, these data seem to suggest that not only this lipophilic region of the binding pocket is separated from the catalytic machinery by a tight opening that can only accommodate linear and/or flat substituents, but also that, immediately after this channel, the subpocket expands and can efficiently lodge bulkier substituents. Putative bound conformations of **9r–v** are reported in Figure S3 in the Supporting Information.

Discovery of NAAA modulators is a quite recent medicinal chemistry field, as few inhibitors of this enzyme have so far been reported in the literature. Here, we aimed at extending the SAR around the series of potent β-lactone NAAA inhibitors. To this objective, we also generated the first 3D QSAR

model in the field, which turned out to be quite robust in terms of both statistical parameters and predictivity, as shown by the 3D QSAR-driven design of novel analogues. We are confident that the present 3D QSAR exploration can also, in a qualitative way, help designing novel structurally unrelated NAAA inhibitors further expanding the chemical diversity in this field.

Conclusions

In this study, we investigated a series of NAAA inhibitors in terms of three-dimensional quantitative structure-activity relationship (3D QSAR), and to the best of our knowledge, this represents the first 3D QSAR model in this field. To this objective, we first expanded the SAR around the 2-methyl-4-oxo-3-oxetanylcarbamic acid esters as NAAA inhibitors, hence investigating the role of previously unexplored structural features on the inhibition of this enzyme. In particular, we further characterized the size and shape of the side chain linked to the carbamic acid function, features that were extensively investigated here for the first time. This eventually led to the discovery of a quite potent NAAA inhibitor, compound **9l**, endowed with single-digit nanomolar activity against this enzyme. In addition, this allowed us to generate a consistent series of analogues that was then utilized to build the 3D QSAR model. The statistical model was obtained using the innovative APF methodology, where discrete features of classic pharmacophores are replaced by continuous, regularly spaced three-dimensional lattices. The 3D QSAR model showed a quite robust statistics and good consistency with docking experiments carried out using a homology built model of NAAA. These promising results prompted us to generate a small set of novel NAAA inhibitors, which were purposely designed and predicted using the 3D QSAR model. The fairly good agreement between theoretical and experimental IC_{50} values for the new 2-methyl-4-oxo-3-oxetanylcarbamic acid esters highlights the good descriptive and predictive power of the model. From a more general standpoint in the field of NAAA inhibitors, the present study shows that an extended and lipophilic moiety could be the ideal pharmacophoric function for substituting the side chain of covalent inhibitors of this enzyme. In conclusion, the present SAR exploration and the 3D QSAR model can help the future design of novel NAAA inhibitors, which can find therapeutic applications in the treatment of pain and inflammation.

Experimental section

a. Chemicals, Materials, and Methods. All the commercial available reagents and solvents were used as purchased from vendors without further purification. Dry solvents (THF, Et_2O, CH_2Cl_2, DMF, DMSO, MeOH) were purchased from Sigma-Aldrich. Optical rotations were measured on a Rudolf Research Analytical Autopol II Automatic polarimeter using a sodium lamp (589 nm) as the light source; concentrations are expressed in g/100 mL using $CHCl_3$ as a solvent and a 1 dm cell. Automated column chromatography purifications were done using a Teledyne ISCO apparatus (Combi*Flash*® R_f) with pre-packed silica gel columns of different sizes (from 4 g up to 120 g). Mixtures of increasing polarity of cyclohexane and ethyl acetate (EtOAc) or cyclohexane and methyl *tert*-butyl ether (MTBE) were used as eluents. NMR experiments were run on a Bruker Avance III 400 system (400.13 MHz for ^1H, and 100.62 MHz for ^{13}C), equipped with a BBI probe and Z-gradients. Spectra were acquired at 300 K, using deuterated dimethylsulfoxide (DMSO-d_6) or deuterated chloroform ($CDCl_3$) as solvents. UPLC–MS analyses were run on a Waters ACQUITY UPLC–MS system consisting of a SQD (Single Quadrupole Detector) Mass Spectrometer equipped with an Electrospray Ionization interface and a Photodiode Array Detector. PDA range was 210-400 nm. Analyses were performed on an ACQUITY UPLC HSS T3 C_{18} column (50x2.1 mm ID, particle size 1.8 μm) with a VanGuard HSS T3 C_{18} pre-column (5x2.1mm ID, particle size 1.8 μm). Mobile phase was either 10 mM NH_4OAc in H_2O at pH 5 adjusted with AcOH (A) and 10 mM NH_4OAc in MeCN-H_2O (95:5) at pH 5. Electrospray ionization in positive and negative mode was applied. Purifications by preparative HPLC–MS were run on a Waters Autopurification system consisting of a 3100 Single Quadrupole Mass Spectrometer equipped with an Electrospray Ionization interface and a 2998 Photodiode Array Detector. HPLC system included a 2747 Sample Manager, 2545 Binary Gradient Module, System Fluidic Organizer and 515 HPLC Pump. PDA range was 210-400 nm. Purifications were performed on a XBridge™ Prep C_{18} OBD column (100x19 mm ID, particle size 5 μm) with a

XBridge™ Prep C_{18} (10x19 mm ID, particle size 5 μm) Guard Cartridge. Mobile phase was 10 mM NH_4OAc in MeCN-H_2O (95:5) at pH 5. Electrospray ionization in positive and negative mode was used. All tested compounds (**9a–v**) showed ≥ 95% purity by NMR and UPLC–MS analysis.

General Procedure for the Synthesis of Carbamates 9r–v (Scheme 1)

Preparation of Activated Alcohols as Alkyl-2-pyridyl Carbonates 5r–v and Alkyl-2-oxopyridine-1-carboxylates 6r–v (Step 1). To a stirred mixture of the suitable alcohol **3r–v** (1.0 eq.) in dry CH_2Cl_2, and under nitrogen atmosphere, DMAP (0.1 eq.) and DPC (1.2 eq.) were added. The reaction mixture was left to react at room temperature for 15 h, then diluted with CH_2Cl_2, washed with a saturated NH_4Cl solution and, subsequently, with a saturated $NaHCO_3$ solution (3x). The combined organic layers were dried over Na_2SO_4, filtered, and concentrated to dryness to give a mixture (ratio 1.6:1) of alkyl-2-pyridyl-carbonate **5r–v** and alkyl-2-oxopyridine-1-carboxylate **6r–v**. The mixture of isomers was not separated and used in the next step without any further purification.

Preparation of β-Hydroxycarboxylic Acids 8r–v (Step 2). To a stirred mixture of D-threonine (1.0 eq.) and $NaHCO_3$ (1.5 eq.) in H_2O (3.5 mL), the isomeric mixture containing the pyridyl carbonate **5r–v** and the 2-oxopyridine-1-carboxylate **6r–v** (1.5 eq.) in THF (3.5 mL) was added. After 15 h at room temperature, the crude was evaporated and subsequently extracted with Et_2O (3x5.0 mL). The aqueous layer was acidified with 2.0 M HCl solution to pH 2-3 and subsequently extracted with EtOAc (3x10 mL). The combined organic layers were dried over Na_2SO_4, filtered, and concentrated to dryness to give the threonine derivatives **8r–v**, which were used in the next step without further purification.

Preparation of carbamates 9r–v (Step 3). To a stirred mixture of threonine derivatives **8r–v** (1.0 eq.) in dry CH_2Cl_2, at 0 °C, and under nitrogen atmosphere, Et_3N (3.0 eq.) and, subsequently, TBTU (1.2 eq.) were added. The mixture was stirred at 0 °C for 1 h and at room temperature for 15 h, then

concentrated, and the crude purified by column chromatography, eluting with cyclohexane:EtOAc (from 100:0 to 0:100) to afford pure **9r**–**v**.

(4-Butylphenyl)methyl-*N*-[(2*S*,3*R*)-2-methyl-4-oxo-oxetan-3-yl]carbamate (9r). The reaction was carried out following the general procedure (Step 3) employing (2*R*,3*S*)-2-[(4-butylphenyl)methoxycarbonylamino]-3-hydroxy-butanoic acid (**8r**) (0.29 g, 0.92 mmol), dry CH_2Cl_2 (28 mL), Et_3N (0.39 mL, 2.77 mmol), and TBTU (0.36 g, 1.10 mmol) to give **9r**. White solid; yield 8% (0.02 g). $[\alpha]^{25}_D$ –17.61 (c 0.1, $CHCl_3$). MS (ESI) *m/z*: 290 $[M–H]^-$, 292 $[M–H]^+$. ^{1}H NMR (400 MHz, DMSO-d_6): δ 0.88 (t, *J* = 7.34 Hz, 3H), 1.22–1.32 (m, 2H), 1.34 (d, *J* = 6.28 Hz, 3H), 1.48–1.59 (m, 2H), 2.57 (t, *J* = 7.65 Hz, 2H), 4.86 (dq, *J* = 6.08, 6.28 Hz, 1H), 5.01 (d, *J* = 12.38 Hz, 1H), 5.06 (d, *J* = 12.10 Hz, 1H), 5.44 (dd, *J* = 6.08, 9.42 Hz, 1H), 7.19 (d, *J* = 7.69 Hz, 2H), 7.27 (d, *J* = 7.77 Hz, 2H), 8.32 (d, *J* = 9.42 Hz, 1H). ^{13}C NMR (101 MHz, DMSO-d_6): δ 14.21, 14.98, 22.15, 33.56, 34.97, 60.41, 66.63, 75.11, 128.58, 128.79, 134.14, 142.76, 156.11, 170.27.

(4-*tert*-Butylphenyl)methyl-*N*-[(2*S*,3*R*)-2-methyl-4-oxo-oxetan-3-yl]carbamate (9s). The reaction was carried out following the general procedure (Step 3) employing (2*R*,3*S*)-2-[(4-*tert*-butylphenyl)methoxycarbonylamino]-3-hydroxy-butanoic acid (**8s**) (0.37 g, 1.21 mmol), dry CH_2Cl_2 (37 mL), Et_3N (0.51 mL, 3.64 mmol), and TBTU (0.47 g, 1.45 mmol) to give **9s**. White solid; yield: 20% (0.07 g). $[\alpha]^{25}_D$ –17.38 (c 0.1, $CHCl_3$). MS (ESI) *m/z*: 290 $[M–H]^-$, 292 $[M–H]^+$. ^{1}H NMR (400 MHz, DMSO-d_6): δ 1.27 (s, 9H), 1.34 (d, *J* = 6.35 Hz, 3H), 4.86 (dq, *J* = 6.08, 6.35 Hz, 1H), 5.01 (d, *J* = 12.15 Hz, 1H), 5.06 (d, *J* = 12.15 Hz, 1H), 5.44 (dd, *J* = 6.08, 9.42 Hz, 1H), 7.26–7.31 (m, 2H), 7.37–7.41 (m, 2H), 8.32 (d, *J* = 9.42 Hz, 1H). ^{13}C NMR (101 MHz, DMSO-d_6): δ 14.55, 31.12, 34.32, 59.96, 66.07, 74.68, 125.20, 127.91, 133.53, 150.64, 155.67, 169.85.

[4-(3-Bromo-2-thienyl)phenyl]methyl-*N*-[(2*S*,3*R*)-2-methyl-4-oxo-oxetan-3-yl]carbamate (**9t**). The reaction was carried out following the general procedure (Step 3) employing (2*R*,3*S*)-2-[[4-(3-bromo-2-

thienyl)phenyl]methoxycarbonylamino]-3-hydroxy-butanoic acid (**8t**) (0.39 g, 0.95 mmol), dry CH_2Cl_2 (40 mL), Et_3N (0.40 mL, 2.85 mmol), and TBTU (0.37 g, 1.14 mmol) to give **9t**. White solid; yield: 13% (0.051 g). $[\alpha]^{25}_D$ –63.21 (c 0.1, $CHCl_3$). MS (ESI) *m/z*: 395 $[M–H]^-$, 397 $[M–H]^+$. ^{1}H NMR (400 MHz, DMSO-d_6): δ 1.36 (d, *J* = 6.32 Hz, 3H), 4.87 (dq, *J* = 6.28 Hz, 1H), 5.11 (d, *J* = 12.89 Hz, 1H), 5.16 (d, *J* = 12.56 Hz, 1H), 5.46 (dd, *J* = 6.06, 9.42 Hz, 1H), 7.19–7.22 (m, 1H), 7.48 (d, *J* = 7.98 Hz, 2H), 7.63 (d, *J* = 7.98 Hz, 2H), 7.71–7.74 (m, 1H), 8.42 (d, *J* = 9.42 Hz, 1H). ^{13}C NMR (101 MHz, DMSO-d_6): 14.54, 59.96, 65.77, 74.65, 107.25, 127.07, 128.28, 128.73, 131.57, 131.91, 136.85, 137.08, 155.56, 169.75.

(5-Methylbenzothiophen-2-yl)methyl-*N*-[(2*S*,3*R*)-2-methyl-4-oxo-oxetan-3-yl]carbamate (**9u)**. The reaction was carried out following the general procedure (Step 3) employing (2*R*,3*S*)-3-hydroxy-2-[(5-methylbenzothiophen-2-yl)methoxycarbonylamino]butanoic acid (**8u**) (0.37 g, 1.15 mmol), dry CH_2Cl_2 (37 mL), Et_3N (0.48 mL, 3.48 mmol), and TBTU (0.45 g, 1.39 mmol) to give **9u**. White solid; yield: 27% (0.095 g). $[\alpha]^{25}_D$ –20.99 (c 0.1, $CHCl_3$). MS (ESI) *m/z*: 304 $[M–H]^-$, 306 $[M–H]^+$. ^{1}H NMR (400 MHz, DMSO-d_6): δ 1.35 (d, *J* = 6.30 Hz, 3H), 2.40 (s, 3H), 4.87 (dq, *J* = 6.08, 6.30 Hz, 1H), 5.32 (d, *J* = 13.20 Hz, 1H), 5.34 (d, *J* = 13.20 Hz, 1H), 5.45 (dd, *J* = 6.07, 9.34 Hz, 1H), 7.19 (dd, *J* = 1.67, 8.23 Hz, 1H), 7.38 (s, 1H), 7.60–7.64 (m, 1H), 7.81 (d, *J* = 8.22 Hz, 1H), 8.44 (d, *J* = 9.34 Hz, 1H). ^{13}C NMR (101 MHz, DMSO-d_6): 14.54, 20.96, 59.99, 61.53, 74.66, 122.22, 123.67, 124.13, 126.42, 133.83, 136.93, 139.19, 139.65, 155.39, 169.64.

Dec-2-ynyl-*N*-[(2*S*,3*R*)-2-methyl-4-oxo-oxetan-3-yl]carbamate (9v). The reaction was carried out following the general procedure (Step 3) employing (2*R*,3*S*)-2-(dec-2-ynoxycarbonylamino)-3-hydroxy-butanoic acid (**8v**) (0.35 g, 1.18 mmol), dry CH_2Cl_2 (35 mL), Et_3N (0.49 mL, 3.56 mmol), and TBTU (0.46 g, 1.42 mmol) to give **9v**. White solid; yield: 26% (0.090 g). $[\alpha]^{25}_D$ –15.83 (c 0.1, $CHCl_3$). MS (ESI) *m/z*: 280 $[M–H]^-$, 282 $[M–H]^+$. ^{1}H NMR (400 MHz, DMSO-d_6): δ 0.83–0.88 (m, 3H), 1.20–

1.37 (m, 12H), 1.38–1.48 (m, 2H), 2.17–2.24 (m, 1H), 4.65 (d, J = 2.62 Hz, 1H), 4.67 (d, J = 2.57 Hz, 1H), 4.86 (dq, J = 6.30 Hz, 1H), 5.43 (dd, J = 6.07, 9.41 Hz, 1H), 8.38 (d, J = 9.41 Hz, 1H). ^{13}C NMR (101 MHz, DMSO-d_6): δ 13.92, 14.48, 17.87, 22.03, 27.88, 28.13, 31.14, 52.98, 59.92, 74.57, 75.11, 87.12, 99.50, 154.98, 169.62.

b. Pharmacology

Rat NAAA in vitro assay.[34] For a detailed description of in-vitro *rat*-NAAA assay, see Supporting Information.

c. Computational Methods

Compounds preparation. For each compound, we generated a two-dimensional representation in which bond orders, tautomeric forms, stereochemistry, hydrogen atoms, and protonation states were manually assigned. Conversion from a two- to a three-dimensional representation was automatically performed by the ICM converting procedure (ICM3.7, Molsoft LLC, San Diego, CA).[41] Cartesian coordinates were translated into internal coordinates and each molecule was assigned the MMFF force field atom types and charges.

Three-dimensional alignment of the training set molecules. We generated our initial structural alignment starting from a rigid template, namely the structure of the transition state model of α-amino β-lactone **2**. Compound **2** transition state was modeled as follows: the 2-methyl-4-oxo-3-oxetanylcarbamic acid ester region was assigned the optimized coordinates that we previously identified by means of quantum chemical calculations.[34] In order to identify a plausible starting conformation of the molecule, we performed an energy optimization on the three torsional angles describing the orientation of the biphenyl moiety by means of the biased probability Monte Carlo (BPMC) stochastic optimizer as implemented in ICM.[42, 43] The vicinity threshold, namely the root-mean-square deviation threshold for the rotatable torsions, was set equal to 15 degrees. In ICM, the

number of Monte Carlo steps is automatically set by an adaptive procedure. After performing Cartesian minimization, we selected the lowest energy conformer appearing compatible with the pocket orientation that was described by Solorzano and coworkers.[32]. Compounds **9a**–**q** were structurally aligned to this rigid template according to the Atomic Property Fields (APF), procedure recently reported and thoroughly described by Totrov.[37] First, we calculated seven continuous three-dimensional grid potentials representing the pharmacophoric features of our template. The grids covered the template plus a 5 Å margin. These APF potentials accounted for: hydrogen bond donor and acceptor propensity, lipophilicity, size, charge, hybridization, and electronegativity. Each molecule to be superimposed to the template was globally optimized within the pre-calculated APF. The intramolecular force-field energy was also taken into account in order to avoid the generation of unrealistically strained conformations. An initial superposition was generated matching the inertia ellipsoid of the molecule in a random conformation with that of the template. Then, an optimization was undertaken using the BPMC method. Torsional variables describing the conformation of flexible rings were sampled explicitly. Thoroughness, namely the parameter that controls the length of the optimization process, was set equal to 1, a value that has been validated to provide a simulation of suitable length.

3D QSAR model. The 3D QSAR model was built starting from the design of a chemical table containing the superimposed compounds and the NAAA inhibitor activity data (Table 1 and Table S1). The APF 3D QSAR methodology as implemented in ICM has been used.[41] For each molecule the 7-component APF were calculated and added together. In order to make the APF model that could provide quantitative prediction of activity for new compounds the proper weight for the contributions of each compound to each APF component has to be defined. Using the activity data for the training set compounds the weights for the contributions of each compound were fitted to reproduce experimental data. The partial least squares (PLS) methodology was used to derive the optimal weights.[44] Once the

weights were derived, partial per-compound potentials were combined into the total weighted QSAR APF and an estimate of activity for a new compound can be performed by a single calculation of the pseudo-energy. The optimal number of latent vectors for PLS was established by leave-one-out cross-validation on the training set. In Table 2 the squared correlation coefficients (R^2) and leave-one-out squared correlation coefficients (Q^2) according to the number of latent vectors are reported.

3D QSAR model validation. We generated a virtual library of β-lactones molecules through the Markush Combinatorial Library tool of ICM using a library of commercially available alcohols reacting with the β-lactone amino group.[41] In this way we automatically created a list of 200 new compounds: their activity data were then derived through the 3D QSAR model. The molecules were then ranked according to their predicted pIC_{50}. We then selected all the compounds with a predicted IC_{50} greater than a pre-specified threshold. Having used **2** as rigid template for the alignment, we set our lower threshold for activity equal to 7.45, corresponding to the potency of the less active biphenyl-bearing derivative (**9o**). Within the selected 23 molecules, only five compounds were then chosen to be synthetized for the subsequent model validation. The choice of these compounds was based on the following criteria: chemical feasibility, good predicted activity data, interesting new chemical features that are not kept by the available known β-lactones molecules.

Figures, Schemes/Structures, and Charts

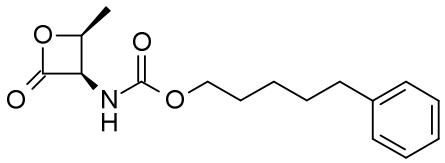

ARN077 (1)

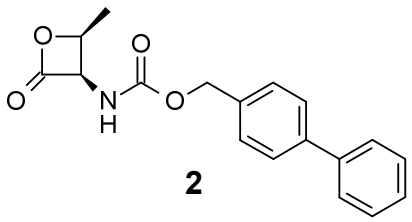

2

Figure 1.

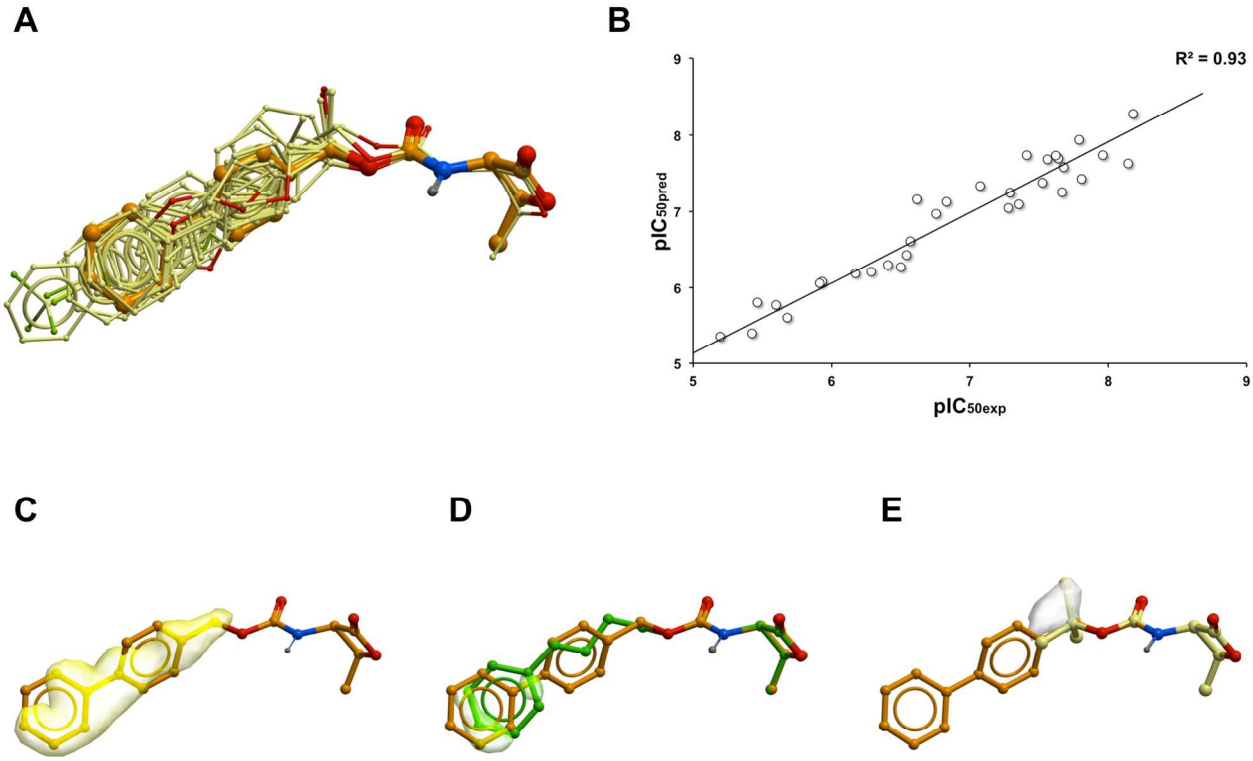

Figure 2.

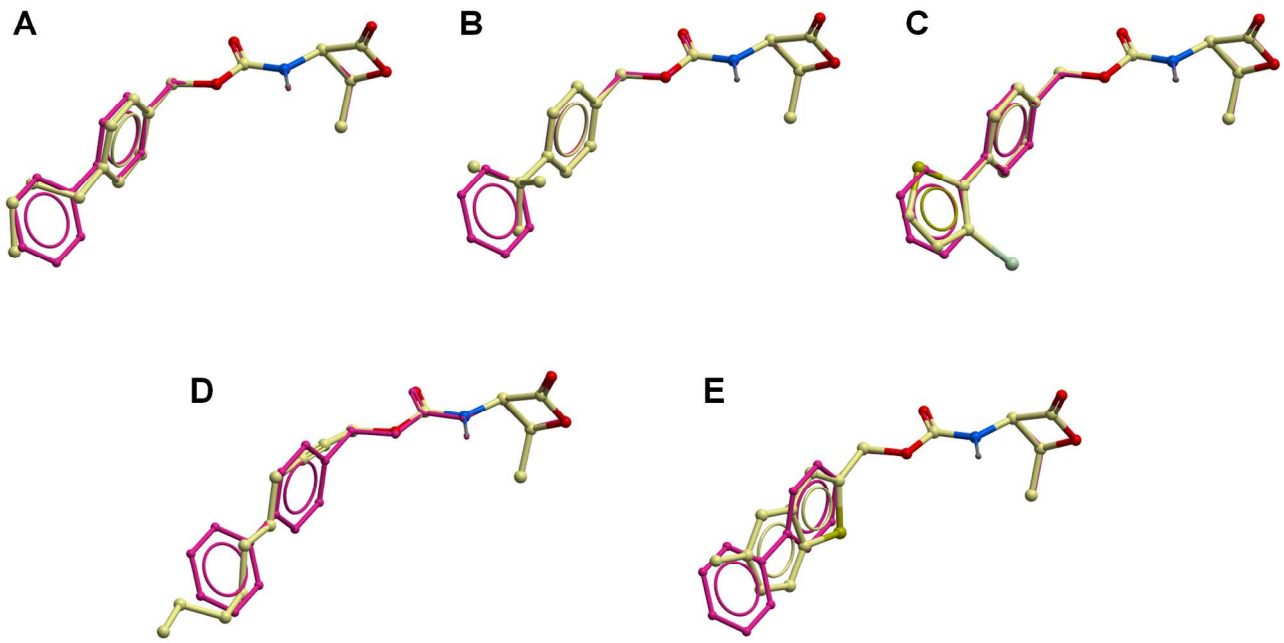

Figure 3

Figure legends

Figure 1. α-Amino β-lactone potent NAAA inhibitors.

Figure 2. A: The overlay of the training set molecules superimposed to compound **2**; B: Correlation plot between pIC_{50exp} and pIC_{50pred}; C: In licorice the 3D structure of **2** is reported. The transparent blobs are the equipotential contours of the lipophilic 3D QSAR APF component. The grey region represents the ideal lipophilic shape for NAAA inhibition. D: In green is reported the 3D structure of **20** superimposed to compound **2**, in orange. The grey blobs represent the equipotential contours of the Sp2 hybridization 3D QSAR APF component. The occupancy of such regions is detrimental for the potency. E: In yellow is reported **16** superimposed to compound **2**, in orange. The grey blobs represent the equipotential contours of the size 3D QSAR APF component. The occupancy of such regions is detrimental for the potency.

Figure 3: The molecules selected for the validation of the 3D QSAR model are shown in yellow, as licorice, superimposed to **2** in pink. A: molecule **9r**, B: molecule **9s**, C: molecule **9t**, D: molecule **9v**, E: molecule **9u**.

Scheme 1. General Synthetic Pathways for the Preparation of 2-Methyl-4-oxo-3-oxetanylcarbamic Acid Esters (**9a**–**v**).

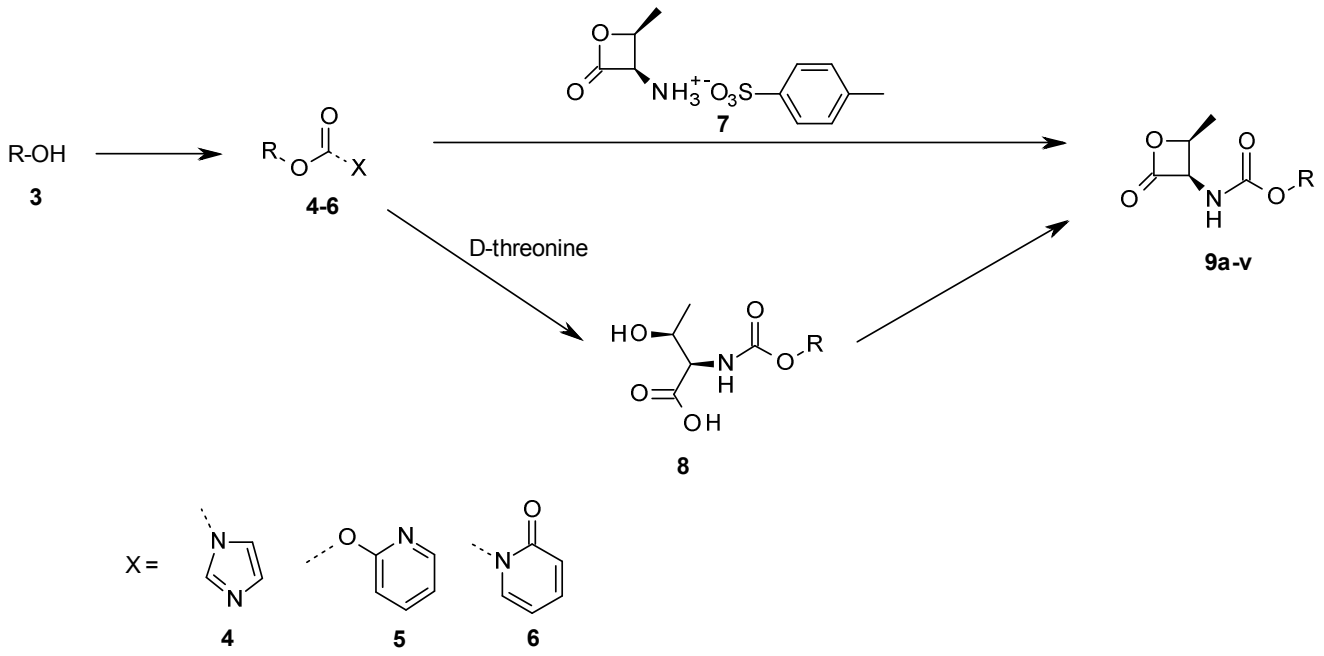

Scheme 2. Syntheses of Alcohols **3c**–**e**,**p**[a]

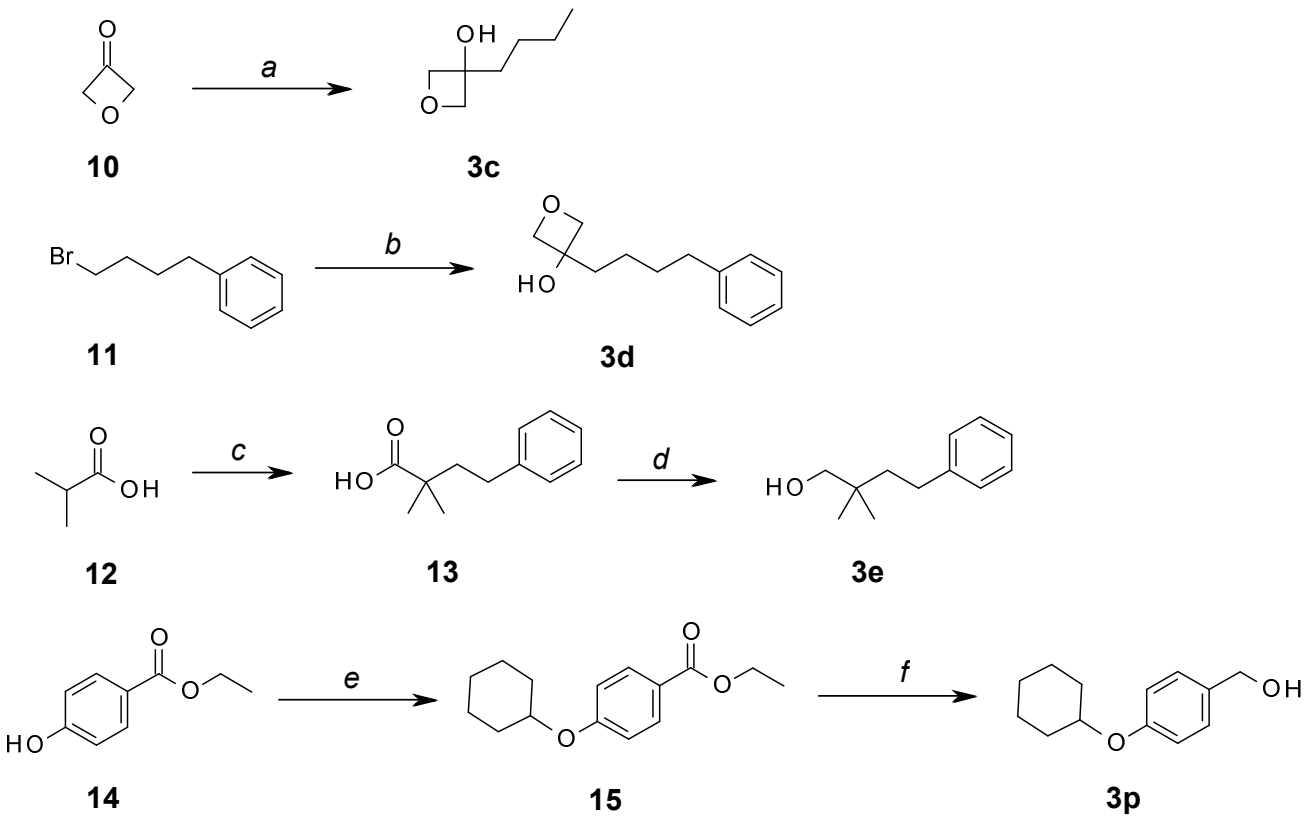

[a]Reagents and conditions: (a) BuLi, THF, −78 °C, 3 h; (b) Li(0), Et_2O, −45 °C, then 0 °C, 3 h, , THF, −78 °C, 3 h; (c) (*i*) diisopropylamine, NaH (60 % in mineral oil), THF, reflux, 15 min, (*ii*) BuLi, 0 °C, 20 min, then, 30-35 °C, 30 min, (*iii*) (2-bromoethyl)-benzene, 0 °C, then, 30-35 °C, 1 h, (*iv*) H_2O, 5-10 °C; (d) $LiAlH_4$, Et_2O, room temperature, 4 h; (e) Cyclohexene, $BF_3{\cdot}OEt_2$, reflux, 2 h; (f) $LiAlH_4$, THF, room temperature, 4 h.

Tables

Table 1. Inhibitory Potencies (IC_{50}) of Compounds **9a**–**q** on Rat NAAA Activity[a]

Compounds	Structure	IC_{50} (μM) ± SD
9a	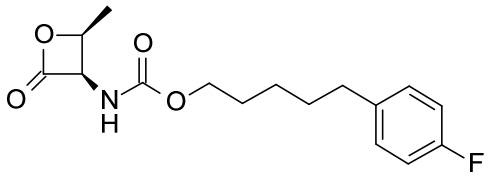	0.24 ± 0.07
9b	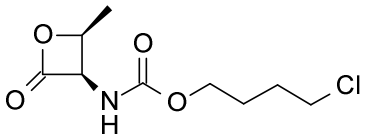	0.288 ± 0.017
9c	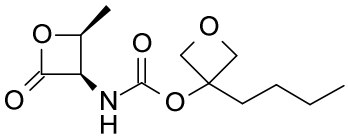	3.76 ± 1.72
9d	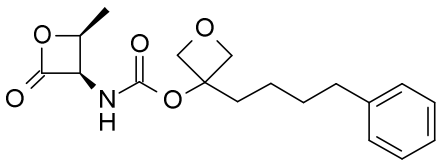	0.52 ± 0.19
9e	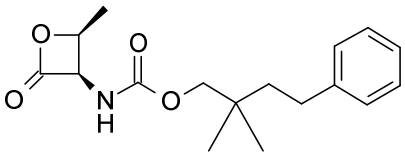	3.43 ± 0.52
9f	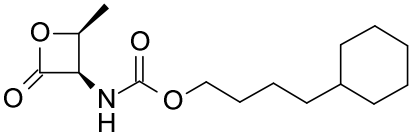	0.02 ± 0.01

9g	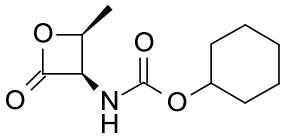	5.42 ± 0.56
9h	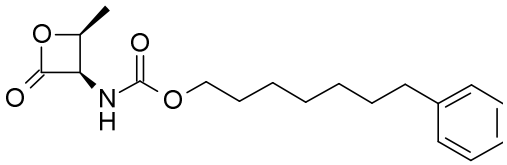	0.039 ± 0.011
9i	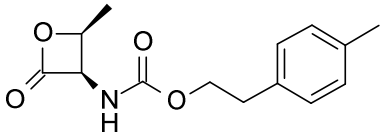	1.22 ± 0.30
9j	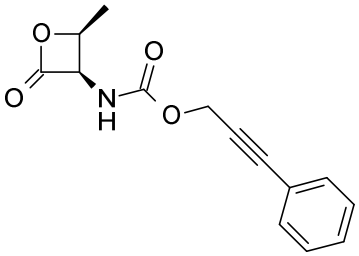	0.02 ± 0.003
9k	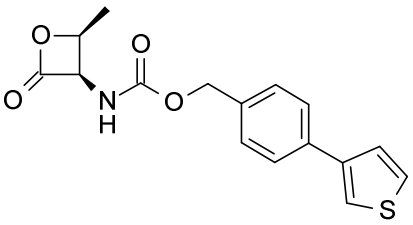	0.022 ± 0.01
9l	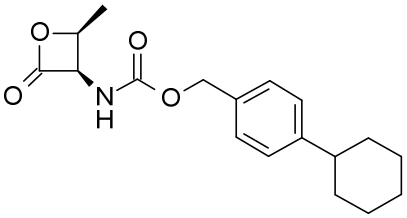	0.007 ± 0.002

9m	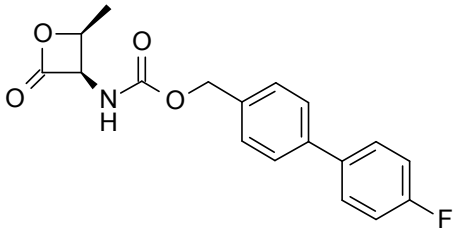	0.011 ± 0.006
9n	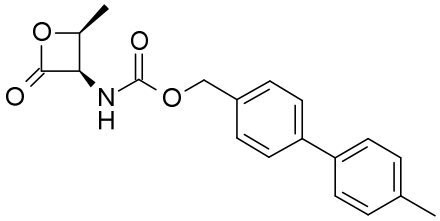	0.029 ± 0.007
9o	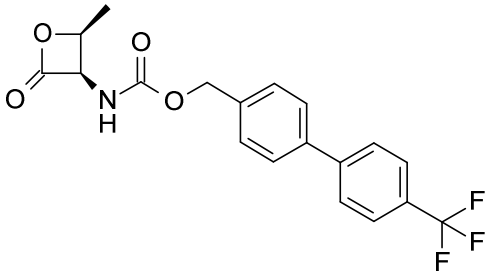	0.036 ± 0.021
9p	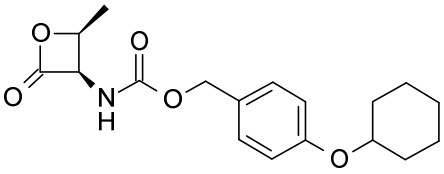	0.023 ± 0.008
9q	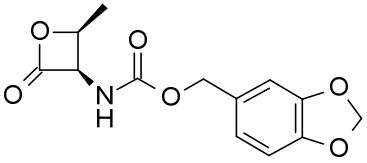	0.176 ± 0.06

[a]IC_{50} values are reported as mean values of three or more determinations.

Table 2. Squared Correlation Coefficients (R^2) and Leave-One-Out Squared Correlation Coefficients (Q^2) According to the Number of Latent Vectors

n. of Latent Vectors	R^2	RMSE[a]	$Q^2_{L.o.o.}$	$RMSE^a_{L.o.o.}$
1	0.37	0.71	0.33	0.74
2	0.59	0.57	0.49	0.64
3	0.63	0.54	0.54	0.61
4	0.70	0.50	0.58	0.61
5	0.84	0.36	0.56	0.60
6	0.93	0.23	0.69	0.51
7	0.95	0.20	0.78	0.43
8	0.96	0.17	0.80	0.42
9	0.97	0.15	0.78	0.44
10	0.98	0.14	0.76	0.47

[a]Root Mean Squared Error

Table 3. Experimental, Predicted, and Leave-One-Out Cross-Validated pIC_{50} Values for the Training Set Compounds.

Compounds	pIC_{50exp}	pIC_{50pred}	$pIC_{50L.O.O.}$
9l	8.18	8.28	8.37
2	8.14	7.63	7.50
9m	7.96	7.74	7.65
9j	7.81	7.43	6.39
28	7.79	7.94	7.99
9k	7.68	7.58	7.50
9f	7.67	7.25	7.05
9p	7.64	7.69	8.00
9n	7.62	7.73	7.77
9o	7.56	7.68	7.71
25	7.52	7.38	7.19
9h	7.41	7.74	7.50
24	7.35	7.09	6.94
26	7.29	7.24	6.65
1	7.28	7.04	6.97
19	7.07	7.34	7.15
27	6.83	7.13	7.02
9q	6.75	6.97	6.93
9a	6.62	7.16	7.30
23	6.57	6.61	6.58
9b	6.54	6.43	6.23
29	6.50	6.27	6.24
20	6.41	6.30	6.37

9d	6.28	6.21	6.30
22	6.17	6.19	6.16
21	5.93	6.08	7.01
9i	5.91	6.06	6.49
17	5.68	5.60	5.12
18	5.60	5.77	6.06
9e	5.46	5.80	6.75
9c	5.42	5.39	5.55
9g	5.27	5.00	4.92
16	5.20	5.35	5.48

Table 4. Inhibitory Potencies (IC_{50}) of QSAR Model Predicted Compounds **9r–v** on Rat NAAA Activity[a]

Compounds	Structure	pIC_{50pred}	Rank	IC_{50} (μM) ± SD	pIC_{50exp}
9r	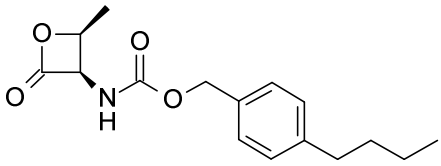	7.61	8th	0.015 ± 0.005	7.82
9s	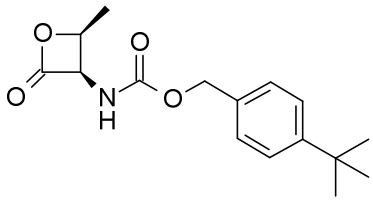	7.60	9th	0.022 ± 0.005	7.66
9t	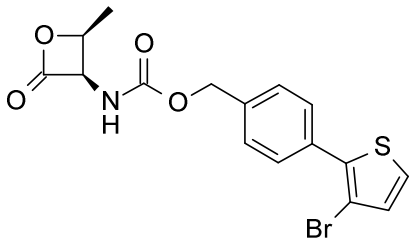	7.55	11th	0.028 ± 0.003	7.55
9u	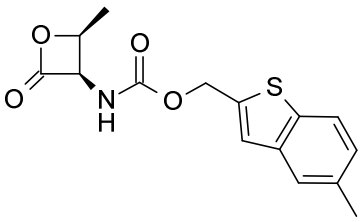	7.46	21st	0.013 ± 0.004	7.89
9v	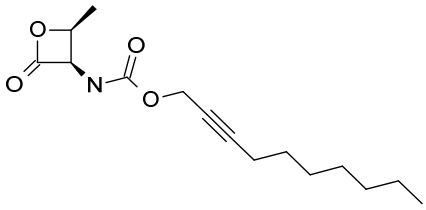	7.45	23rd	0.077 ± 0.029	7.11

[a] IC_{50} values are reported as mean values of three or more determinations.

Supporting Information

Supporting Information Available: Detailed experimental procedures, analytical and spectroscopical data of intermediate and final compounds, ^{1}H and ^{13}C NMR spectra of compounds **9r–v** are reported. In-vitro pharmacology procedures, and additional computational details on the 3D QSAR predicted activity are reported. This material is available free of charge via the Internet at http://pubs.acs.org.

AUTHOR INFORMATION

Corresponding Authors

For G.B.: phone, +39-010-71781522; e-mail, giovanni.bottegoni@iit.it.

For F.B.: phone, +39-010-71781235; fax, +39-010-71781228; e-mail, fabio.bertozzi@iit.it

Author Contributions

[#]S.P and A.B. contributed equally to this work.

Notes

The authors declare the following competing financial interest(s): Piomelli, D.; Bandiera, T.; Bertozzi, F.; Ponzano, S. are inventors in the patent application WO2013078430 protecting the class of compounds disclosed in this paper.

Acknowledgments

The authors wish to thank Sine Mandrup Bertozzi for reverse phase HPLC purifications, Luca Goldoni for NMR technical support, and Silvia Venzano for compounds handling.

Abbreviations Used

FAEs, fatty acid ethanolamides; OEA, oleoylethanolamide; PEA, palmitoylethanolamide; NAAA, *N*-acylethanolamine acid amidase; FAAH, fatty acid amide hydrolase; CBAH, conjugated bile acid hydrolase; PPAR-α, peroxisome proliferator-activated receptor-α; (*S*)-OOPP, (*S*)-*N*-(2-oxo-3-oxetanyl)-3-phenylpropionamide; DPC, di-2-pyridyl carbonate; DMAP, 4-dimethylaminopyridine; APF, atomic property field; PLS, partial least square.

References

1. Calignano, A.; La Rana, G.; Giuffrida, A.; Piomelli, D. Control of Pain Initiation by Endogenous Cannabinoids. *Nature* **1998**, *394*, 277-281.

2. LoVerme, J.; Russo, R.; La Rana, G.; Fu, J.; Farthing, J.; Mattace-Raso, G.; Meli, R.; Hohmann, A.; Calignano, A.; Piomelli, D. Rapid Broad-Spectrum Analgesia through Activation of Peroxisome Proliferator-Activated Receptor-Alpha. *J. Pharmacol. Exp. Ther.* **2006**, *319*, 1051-1061.

3. Sasso, O.; Moreno-Sanz, G.; Martucci, C.; Realini, N.; Dionisi, M.; Mengatto, L.; Duranti, A.; Tarozzo, G.; Tarzia, G.; Mor, M.; Bertorelli, R.; Reggiani, A.; Piomelli, D. Antinociceptive Effects of the *N*-Acylethanolamine Acid Amidase Inhibitor ARN077 in Rodent Pain Models. *Pain* **2013**, *154*, 350-360.

4. Lo Verme, J.; Fu, J.; Astarita, G.; La Rana, G.; Russo, R.; Calignano, A.; Piomelli, D. The Nuclear Receptor Peroxisome Proliferator-Activated Receptor-Alpha Mediates the Anti-Inflammatory Actions of Palmitoylethanolamide. *Mol. Pharmacol.* **2005**, *67*, 15-19.

5. Melis, M.; Pillolla, G.; Luchicchi, A.; Muntoni, A. L.; Yasar, S.; Goldberg, S. R.; Pistis, M. Endogenous Fatty Acid Ethanolamides Suppress Nicotine-Induced Activation of Mesolimbic Dopamine Neurons through Nuclear Receptors. *J. Neurosci.* **2008**, *28*, 13985-13994.

6. Rodriguez de Fonseca, F.; Navarro, M.; Gomez, R.; Escuredo, L.; Nava, F.; Fu, J.; Murillo-Rodriguez, E.; Giuffrida, A.; LoVerme, J.; Gaetani, S.; Kathuria, S.; Gall, C.; Piomelli, D. An Anorexic Lipid Mediator Regulated by Feeding. *Nature* **2001**, *414*, 209-212.

7. Fu, J.; Gaetani, S.; Oveisi, F.; Lo Verme, J.; Serrano, A.; Rodriguez De Fonseca, F.; Rosengarth, A.; Luecke, H.; Di Giacomo, B.; Tarzia, G.; Piomelli, D. Oleylethanolamide Regulates

Feeding and Body Weight through Activation of the Nuclear Receptor PPAR-Alpha. *Nature* **2003**, *425*, 90-93.

8. Berdyshev, E.; Boichot, E.; Corbel, M.; Germain, N.; Lagente, V. Effects of Cannabinoid Receptor Ligands on LPS-Induced Pulmonary Inflammation in Mice. *Life Sci.* **1998**, *63*, PL125-PL129.

9. D'Agostino, G.; La Rana, G.; Russo, R.; Sasso, O.; Iacono, A.; Esposito, E.; Raso, G. M.; Cuzzocrea, S.; Lo Verme, J.; Piomelli, D.; Meli, R.; Calignano, A. Acute Intracerebroventricular Administration of Palmitoylethanolamide, an Endogenous Peroxisome Proliferator-Activated Receptor-Alpha Agonist, Modulates Carrageenan-Induced Paw Edema in Mice. *J. Pharmacol. Exp. Ther.* **2007**, *322*, 1137-1143.

10. Mazzari, S.; Canella, R.; Petrelli, L.; Marcolongo, G.; Leon, A. *N*-(2-Hydroxyethyl)hexadecanamide is Orally Active in Reducing Edema Formation and Inflammatory Hyperalgesia by Down-Modulating Mast Cell Activation. *Eur. J. Pharmacol.* **1996**, *300*, 227-236.

11. Calignano, A.; La Rana, G.; Piomelli, D. Antinociceptive Activity of the Endogenous Fatty Acid Amide, Palmitylethanolamide. *Eur. J. Pharmacol.* **2001**, *419*, 191-198.

12. Darmani, N. A.; Izzo, A. A.; Degenhardt, B.; Valenti, M.; Scaglione, G.; Capasso, R.; Sorrentini, I.; Di Marzo, V. Involvement of the Cannabimimetic Compound, *N*-Palmitoyl-ethanolamine, in Inflammatory and Neuropathic Conditions: Review of the Available Pre-Clinical Data, and First Human Studies. *Neuropharmacology* **2005**, *48*, 1154-1163.

13. Petrosino, S.; Cristino, L.; Karsak, M.; Gaffal, E.; Ueda, N.; Tuting, T.; Bisogno, T.; De Filippis, D.; D'Amico, A.; Saturnino, C.; Orlando, P.; Zimmer, A.; Iuvone, T.; Di Marzo, V. Protective Role of Palmitoylethanolamide in Contact Allergic Dermatitis. *Allergy* **2010**, *65*, 698-711.

14. Kemeny, L.; Koreck, A.; Kis, K.; Kenderessy-Szabo, A.; Bodai, L.; Cimpean, A.; Paunescu, V.; Raica, M.; Ghyczy, M. Endogenous Phospholipid Metabolite Containing Topical Product Inhibits Ultraviolet Light-Induced Inflammation and DNA Damage in Human Skin. *Skin Pharmacol. Physiol.* **2007**, *20*, 155-161.

15. Hesselink, J. M.; Hekker, T. A. Therapeutic Utility of Palmitoylethanolamide in the Treatment of Neuropathic Pain Associated with Various Pathological Conditions: a Case Series. *J. Pain Res.* **2012**, *5*, 437-442.

16. Khasabova, I. A.; Xiong, Y.; Coicou, L. G.; Piomelli, D.; Seybold, V. Peroxisome Proliferator-Activated Receptor Alpha Mediates Acute Effects of Palmitoylethanolamide on Sensory Neurons. *J. Neurosci.* **2012**, *32*, 12735-12743.

17. Desarnaud, F.; Cadas, H.; Piomelli, D. Anandamide Amidohydrolase Activity in Rat Brain Microsomes. Identification and Partial Characterization. *J. Biol. Chem.* **1995**, *270*, 6030-6035.

18. Ueda, N.; Yamanaka, K.; Yamamoto, S. Purification and Characterization of an Acid Amidase Selective for *N*-Palmitoylethanolamine, a Putative Endogenous Anti-Inflammatory Substance. *J. Biol. Chem.* **2001**, *276*, 35552-35557.

19. Tsuboi, K.; Sun, Y. X.; Okamoto, Y.; Araki, N.; Tonai, T.; Ueda, N. Molecular Characterization of *N*-Acylethanolamine-hydrolyzing Acid Amidase, a Novel Member of the Choloylglycine Hydrolase Family with Structural and Functional Similarity to Acid Ceramidase. *J. Biol. Chem.* **2005**, *280*, 11082-11092.

20. Tsuboi, K.; Takezaki, N.; Ueda, N. The *N*-Acylethanolamine-hydrolyzing Acid Amidase (NAAA). *Chem. Biodivers.* **2007**, *4*, 1914-1925.

21. Bandiera, T.; Ponzano, S.; Piomelli, D. Advances in the Discovery of *N*-Acylethanolamine Acid Amidase Inhibitors. *Pharmacol. Res.* **2014**, *86*, 11-17.

22. Fiasella, A.; Nuzzi, A.; Summa, M.; Armirotti, A.; Tarozzo, G.; Tarzia, G.; Mor, M.; Bertozzi, F.; Bandiera, T.; Piomelli, D. 3-Aminoazetidin-2-one Derivatives as *N*-Acylethanolamine Acid Amidase (NAAA) Inhibitors Suitable for Systemic Administration. *ChemMedChem* **2014**, *9*, 1602-1614.

23. Vandevoorde, S.; Tsuboi, K.; Ueda, N.; Jonsson, K. O.; Fowler, C. J.; Lambert, D. M. Esters, Retroesters, and a Retroamide of Palmitic Acid: Pool for the First Selective Inhibitors of *N*-Palmitoylethanolamine Selective Acid Amidase. *J. Med. Chem.* **2003**, *46*, 4373-4376.

24. Saturnino, C.; Petrosino, S.; Ligresti, A.; Palladino, C.; De Martino, G.; Bisogno, T.; Di Marzo, V. Synthesis and Biological Evaluation of New Potential Inhibitors of *N*-Acylethanolamine Hydrolyzing Acid Amidase. *Bioorg. Med. Chem. Lett.* **2010**, *20*, 1210-1213.

25. Tsuboi, K.; Hilligsmann, C.; Vandevoorde, S.; Lambert, D. M.; Ueda, N. *N*-Cyclohexanecarbonylpentadecylamine: a Selective Inhibitor of the Acid Amidase Hydrolysing *N*-Acylethanolamines, as a Tool to Distinguish Acid Amidase from Fatty Acid Amide Hydrolase. *Biochem. J.* **2004**, *379*, 99-106.

26. Yamano, Y.; Tsuboi, K.; Hozaki, Y.; Takahashi, K.; Jin, X. H.; Ueda, N.; Wada, A. Lipophilic Amines as Potent Inhibitors of *N*-Acylethanolamine-hydrolyzing Acid Amidase. *Bioorg. Med. Chem.* **2012**, *20*, 3658-3665.

27. Li, Y.; Yang, L.; Chen, L.; Zhu, C.; Huang, R.; Zheng, X.; Qiu, Y.; Fu, J. Design and Synthesis of Potent *N*-Acylethanolamine-hydrolyzing Acid Amidase (NAAA) Inhibitor as Anti-Inflammatory Compounds. *PLoS One* **2012**, *7*, e43023.

28. Ueda, N.; Tsuboi, K.; Lambert, D. M. A Second *N*-Acylethanolamine Hydrolase in Mammalian Tissues. *Neuropharmacology* **2005**, *48*, 1079-1085.

29. Ueda, N.; Tsuboi, K.; Uyama, T. N-Acylethanolamine Metabolism with Special Reference to *N*-Acylethanolamine-hydrolyzing Acid Amidase (NAAA). *Prog. Lipid Res.* **2010**, *49*, 299-315.

30. Zhao, L. Y.; Tsuboi, K.; Okamoto, Y.; Nagahata, S.; Ueda, N. Proteolytic Activation and Glycosylation of *N*-Acylethanolamine-hydrolyzing Acid Amidase, a Lysosomal Enzyme Involved in the Endocannabinoid Metabolism. *Biochim. Biophys. Acta* **2007**, *1771*, 1397-1405.

31. Solorzano, C.; Zhu, C.; Battista, N.; Astarita, G.; Lodola, A.; Rivara, S.; Mor, M.; Russo, R.; Maccarrone, M.; Antonietti, F.; Duranti, A.; Tontini, A.; Cuzzocrea, S.; Tarzia, G.; Piomelli, D. Selective *N*-Acylethanolamine-hydrolyzing Acid Amidase Inhibition Reveals a Key Role for Endogenous Palmitoylethanolamide in Inflammation. *Proc. Natl. Acad. Sci. U.S.A.* **2009**, *106*, 20966-20971.

32. Solorzano, C.; Antonietti, F.; Duranti, A.; Tontini, A.; Rivara, S.; Lodola, A.; Vacondio, F.; Tarzia, G.; Piomelli, D.; Mor, M. Synthesis and Structure-Activity Relationships of *N*-(2-oxo-3-oxetanyl)amides as *N*-Acylethanolamine-hydrolyzing Acid Amidase Inhibitors. *J. Med. Chem.* **2010**, *53*, 5770-5781.

33. Duranti, A.; Tontini, A.; Antonietti, F.; Vacondio, F.; Fioni, A.; Silva, C.; Lodola, A.; Rivara, S.; Solorzano, C.; Piomelli, D.; Tarzia, G.; Mor, M. *N*-(2-Oxo-3-oxetanyl)carbamic Acid Esters as *N*-Acylethanolamine Acid Amidase Inhibitors: Synthesis and Structure-Activity and Structure-Property Relationships. *J. Med. Chem.* **2012**, *55*, 4824-4836.

34. Ponzano, S.; Bertozzi, F.; Mengatto, L.; Dionisi, M.; Armirotti, A.; Romeo, E.; Berteotti, A.; Fiorelli, C.; Tarozzo, G.; Reggiani, A.; Duranti, A.; Tarzia, G.; Mor, M.; Cavalli, A.; Piomelli, D.;

Bandiera, T. Synthesis and Structure-Activity Relationship (SAR) of 2-Methyl-4-oxo-3-oxetanylcarbamic Acid Esters, a Class of Potent *N*-Acylethanolamine Acid Amidase (NAAA) Inhibitors. *J. Med. Chem.* **2013**, *56*, 6917-6934.

35. Vitale, R.; Ottonello, G.; Petracca, R.; Bertozzi, S. M.; Ponzano, S.; Armirotti, A.; Berteotti, A.; Dionisi, M.; Cavalli, A.; Piomelli, D.; Bandiera, T.; Bertozzi, F. Synthesis, Structure-Activity, and Structure-Stability Relationships of 2-Substituted-*N*-(4-oxo-3-oxetanyl) *N*-Acylethanolamine Acid Amidase (NAAA) Inhibitors. *ChemMedChem* **2014**, *9*, 323-336.

36. Armirotti, A.; Romeo, E.; Ponzano, S.; Mengatto, L.; Dionisi, M.; Karacsonyi, C.; Bertozzi, F.; Garau, G.; Tarozzo, G.; Reggiani, A.; Bandiera, T.; Tarzia, G.; Mor, M.; Piomelli, D. Beta-Lactones Inhibit *N*-Acylethanolamine Acid Amidase by *S*-Acylation of the Catalytic *N*-Terminal Cysteine. *ACS Med. Chem. Lett.* **2012**, *3*, 422-426.

37. Totrov, M. Atomic Property Fields: Generalized 3D Pharmacophoric Potential for Automated Ligand Superposition, Pharmacophore Elucidation and 3D QSAR. *Chem. Biol. Drug Des.* **2008**, *71*, 15-27.

38. Lu, Q.; Wang, D. S.; Chen, C. S.; Hu, Y. D.; Chen, C. S. Structure-Based Optimization of Phenylbutyrate-Derived Histone Deacetylase Inhibitors. *J. Med. Chem.* **2005**, *48*, 5530-5535.

39. Kloss, F.; Lincke, T.; Hertweck, C. Highly Efficient Total Synthesis of the Clostridium-Derived anti-MRSA Antibiotic Closthioamide. *Eur. J. Org. Chem.* **2011**, 1429-1431.

40. Verma, J.; Khedkar, V. M.; Coutinho, E. C. 3D-QSAR in Drug Design - a Review. *Curr. Top. Med. Chem.* **2010**, *10*, 95-115.

41. Abagyan, R.; Orry, A.; Raush, E.; Totrov, M. *ICM Manual 3.7*; Molsoft LCC: San Diego, CA, **2013**.

42. Abagyan, R.; Totrov, M. Biased Probability Monte Carlo Conformational Searches and Electrostatic Calculations for Peptides and Proteins. *J. Mol. Biol.* **1994**, *235*, 983-1002.

43. Totrov, M.; Abagyan, R. Protein-Ligand Docking as an Energy Optimization Problem. In *Drug-Receptor Thermodynamics: Introduction and Applications*; Raffa, R. B., Eds.; Wiley: New York, 2001; pp 603-624.

44. Wold, S.; Johansson, E.; Cocchi, M. PLS: Partial Least Squares Projections to Latent Structures. In *3D QSAR in Drug Design: Theory, Methods and Applications*; Kubinyi, H., Eds.; ESCOM Science Publishers: Leiden, 1993; pp 523-550.

Table of Contents Graphic

Synthesis, Biological Evaluation, and 3D QSAR Study of 2-Methyl-4-oxo-3-oxetanylcarbamic Acid Esters as *N*-Acylethanolamine Acid Amidase (NAAA) Inhibitors

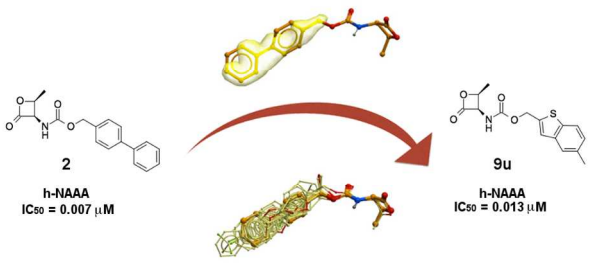

Stefano Ponzano, Anna Berteotti, Rita Petracca, Romina Vitale, Luisa Mengatto, Tiziano Bandiera, Giovanni Bottegoni, Fabio Bertozzi, Daniele Piomelli, Andrea Cavalli

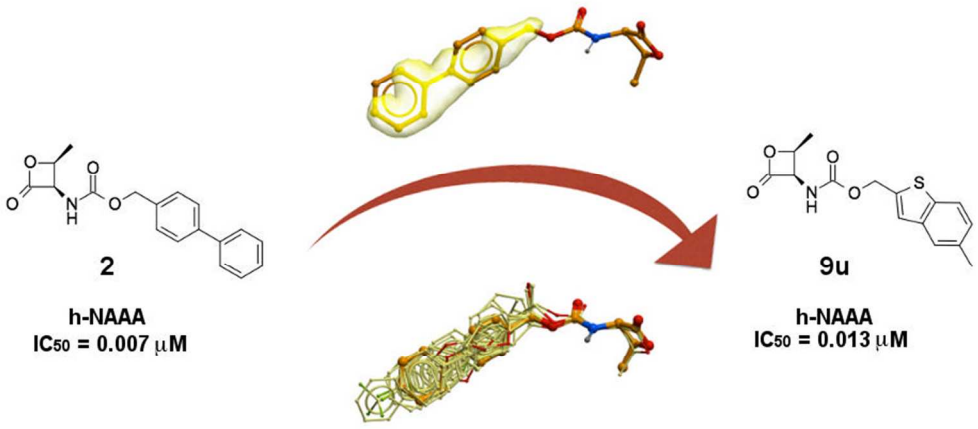

79x36mm (300 x 300 DPI)

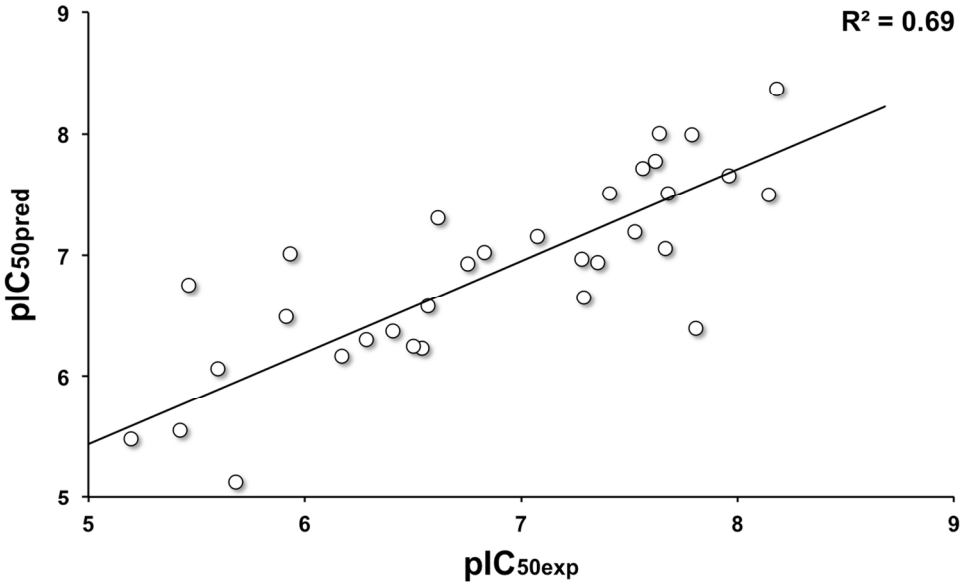

Figure S1: Correlation plot between the experimental pIC50 and the leave-one-out cross-validated pIC50.
177x108mm (300 x 300 DPI)

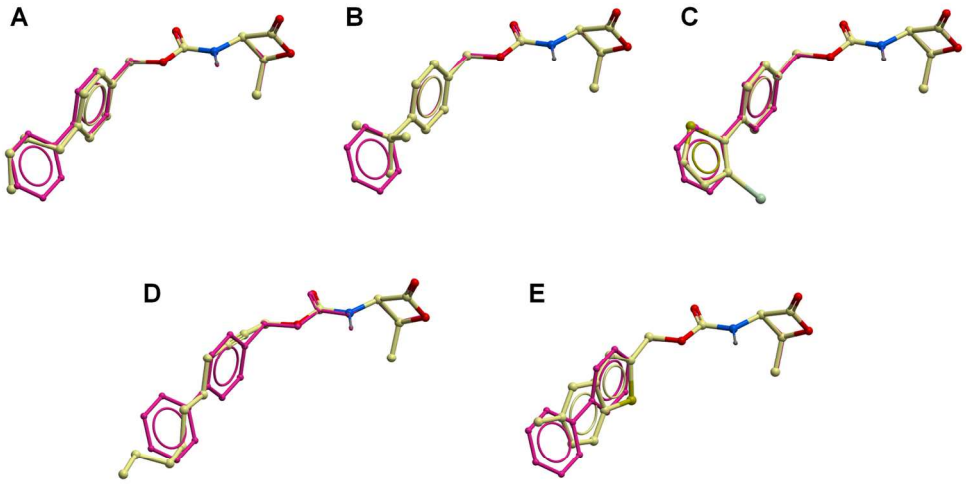

Figure 3: The molecules selected for the validation of the 3D QSAR model are shown in yellow, as licorice, superimposed to 2 in pink. A: molecule 9r, B: molecule 9s, C: molecule 9t, D: molecule 9v, E: molecule 9u. 177x123mm (300 x 300 DPI)

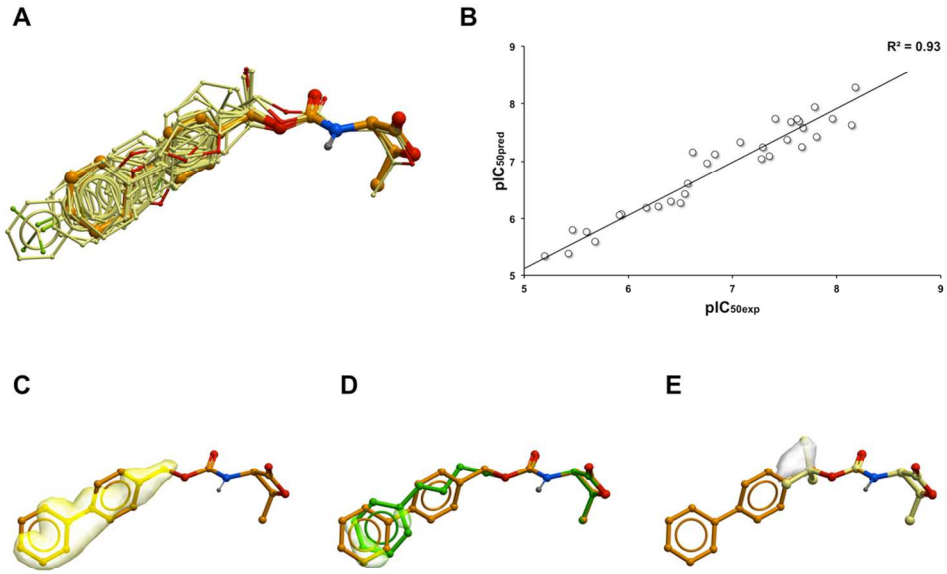

Figure 2. A: The overlay of the training set molecules superimposed to compound 2; B: Correlation plot between pIC50exp and pIC50pred; C: In licorice the 3D structure of 2 is reported. The transparent blobs are the equipotential contours of the lipophilic 3D QSAR APF component. The grey region represents the ideal lipophilic shape for NAAA inhibition. D: In green is reported the 3D structure of 20 superimposed to compound 2, in orange. The grey blobs represent the equipotential contours of the Sp2 hybridization 3D QSAR APF component. The occupancy of such regions is detrimental for the potency. E: In yellow is reported 16 superimposed to compound 2, in orange. The grey blobs represent the equipotential contours of the size 3D QSAR APF component. The occupancy of such regions is detrimental for the potency
177x123mm (300 x 300 DPI)